Hydrogen Cracking in SiO_2: Kinetics for H_2 Dissociation at Silicon Dangling Bonds†

Henry A. Kurtz*,‡ and Shashi P. Karna§

Department of Chemistry, CROMIUM, University of Memphis, Memphis, Tennessee 38152 and Air Force Research Laboratory, 3550 Aberdeen Ave, SE, Kirtland AFB, New Mexico 87117-5776

Received: October 27, 1999; In Final Form: March 9, 2000

The passivation of silicon dangling bond defects by H_2 is an important reaction in Si/SiO_2 devices. The dangling bonds studied in this work are those in the *a*-SiO_2 layers, prototype E′ centers. Experimental estimates of the activation energy of this process are 0.3−0.4 eV, but theoretical calculations give energy barriers that are much larger, around 0.7−0.8 eV. It was suggested that the lack of tunneling in the energy barrier calculations is responsible for the overestimation. This paper is a systematic examination of this reaction, which includes tunneling corrections using the direct dynamics variational transition state theory. The inclusion of this effect is shown to provide an Arrhenius activation energy in good accord with the experimental values.

I. Introduction

Hydrogen is known to play an important role in both passivation of defects in SiO_2 and in the generation of new defect sites. These reactions play important roles in metal-oxide semiconductor device failure and in developing radiation hardened devices. A very important set of defects are silicon atoms with one unpaired electron (a so-called dangling bond), and these are known generically as E′ centers.[1] The annealing of E′ centers has been shown to be qualitatively the same in thermal SiO_2 on Si wafers and in bulk vitreous silica.[2] Li et al.[3] demonstrated that H_2 is an important annealing agent, along with H_2O and O_2, and further studied the kinetics of E′ center annealing by H_2. They demonstrated that a simple diffusion-limited model did not fit the results for H_2 as it does for H_2O. They interpreted their data in terms of a working hypothesis for E′ center passivation as $H_2 + {\cdot}Si(O\sim)_3 \rightarrow {\cdot}H + HSi(O\sim)_3$, where the wavy lines represent the connections into the bulk SiO_2. Using a rate expression consistent with the above reaction, Li et al. obtained rate constants at several different temperatures and fit the data to an Arrhenius plot to obtain an activation energy for the process of 0.3 eV. This is much lower than the 1.66 eV activation energy for the similar H_2 reaction at Si dangling orbitals at a silicon surface at the Si/SiO_2 interface, known as P_b centers.[4] It is also close to the activation energy of 0.38 eV associated with H_2 diffusion in SiO_2.[5] A more recent study by Radzig et al.[6] estimated the activation energy for this process to be 0.40 eV.

Earlier theoretical work by Edwards[7,8] estimated the activation energy of the above process to be around 0.7 eV larger than the experimental value. It was suggested that the discrepancy may arise because quantum tunneling effects are important for H_2 reactions. Edwards estimated these tunneling effects and obtained the very low activation of 0.1 eV. It is this discrepancy that we will attempt to clarify in this paper.

II. Energetics

The first model for the passivation or cracking reaction studied in this work is the small cluster reaction

$$H_2 + {\cdot}Si(OH)_3 \rightarrow {\cdot}H + HSi(OH)_3$$

which is one of the cluster models used by Edwards.[4] The energetics of the model reaction is studied by calculating the molecular structure and energies of the reactants and products. The reactants and products are characterized by having all positive harmonic vibrational frequencies (i.e., all positive second derivatives of the energy with respect to atomic motion). The energetic barrier to the reaction is found by calculating the molecular structure and energy corresponding to the highest point on the minimum energy pathway connecting the reactants and products. This point is called the transition state or transition structure (TS). The TS corresponds to a saddle point on the potential energy surface and is characterized by having one, and only one, imaginary vibrational frequency (i.e., having one negative eigenvalue of the matrix of energy second derivatives).

This model reaction is small enough that a good test of the methods for obtaining energies and structures can be performed. Initially, for each of the reactants, products, and transition structures, the molecular structures were optimized using the unrestricted Hartree−Fock method (UHF) for the radical, open-shell species and restricted Hartree−Fock (RHF) for the closed-shell species. The 6-31G** one-electron basis set was used.[9] For this study, the 6-31G** basis set used for Si was the one developed by Gordon and co-workers.[10] The resulting structures for ${\cdot}Si(OH)_3$, $HSi(OH)_3$, and $H-H-Si(OH)_3$ are shown in Figure 1. This model differs from the previous same-sized model of Edwards[7] in that no artificial symmetry was imposed. Each of the species other than H and H_2 are of C_1 point group symmetry (no symmetry constraints). At this level of theory, the energy of the reaction ($E_{products} - E_{reactants}$) is −0.017 eV (−0.402 kcal/mol), which is slightly exothermic. The activation energy for the reaction calculated as the energy difference $E_{TS} - E_{reactants}$ is 0.795 eV (18.341 kcal/mol). This value is considerably larger than the experimental values of 0.3−0.4 eV.

Table 1 shows the energy of reaction obtained using improved one-electron basis sets and/or adding electron correlation effects via second-order Møller−Plesset perturbation theory (MP2). In this table and the rest of this report, the notation Method1-(basis1)//Method2(basis2) refers to calculations done using method 1 (either Hartree−Fock or MP2) with basis set 1 at an

† Part of the special issue "Electronic and Nonlinear Optical Materials: Theory and Modeling".

‡ Department of Chemistry, University of Memphis.

§ Air Force Research Laboratory.

10.1021/jp993804d CCC: $19.00
Published on Web 04/20/2000

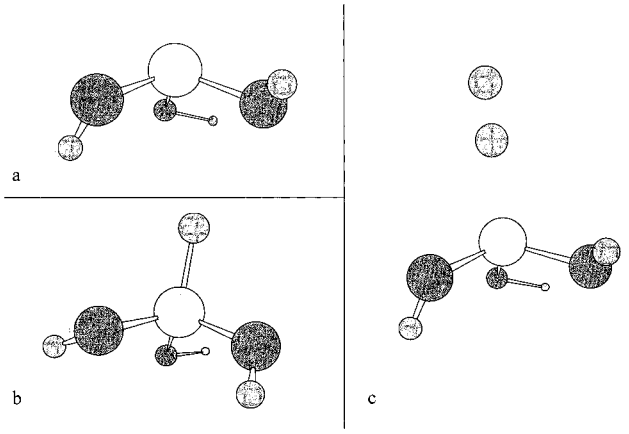

Figure 1. Calculated Structures for (a) the reactant $Si(OH)_3$, (b) the product $HSi(OH)_3$, and (c) the transition state $H-H-Si(OH)_3$.

TABLE 1: Reaction Energies for $H_2 + \cdot Si(OH)_3$ $\cdot H + HSi(OH)_3$

	reaction energy	
method (energy/geometry)	eV	kcal/mol
UHF(6-31G**)//UHF(6-31G**)	−0.017	−0.40
UHF(6-311G**)//UHF(6-31G**)	−0.067	−1.54
UHF(6-31G**++)//UHF(6-31G**)	0.062	1.44
UHF(6-31G**)//MP2(6-31G**)	−0.024	−0.55
UHF(6-31G**++)//MP2(6-31G**)	0.056	1.29
MP2(6-31G**)//UHF(6-31G**)	0.187	4.31
MP2(6-311G**)//UHF(6-31G**)	0.098	2.26
MP2(6-31G**++)//UHF(6-31G**)	0.266	6.14
MP2(6-31G**)//MP2(6-31G**)	0.193	4.44
MP2(6-31G**++)//MP2(6-31G**)	0.276	6.36

optimized geometry obtained from method 2 with basis set 2. For example, MP2(6-31G**++)//UHF(6-31G**) uses energies obtained from an MP2 calculation using the 6-31G**++ basis set with the molecular geometries from an UHF calculation using a 6-31G** basis set. The structure and energy results presented in this report were obtained using the GAMESS[11] and GAUSSIAN94[12] programs.

Basis set improvements, as illustrated by the first three rows of Table 1, have contradictory effects, but the magnitudes are very small. In the 6-311G** basis set, the size of the one-electron basis used to describe the valence shell is increased and, in the 6-31G**++ basis set, extra diffuse functions were added to each atom. The inclusion of electron correlation at the MP2 level has a larger effect on the results, changing the essentially energy-neutral reaction into one that is definitely endothermic. However, the resulting reaction energy is still quite small. Table 1 also illustrates that the overall energetics of this reaction are not particularly sensitive to geometry; results based on UHF structures agree quite well with results based on MP2 structures. Allendorf et al.[13] obtained an MP4/6-31G* estimate of $\Delta H°$ (298 K) of 3.30 kcal/mol, close to the MP2 estimate here.

The main quantities of interest in this study are the activation energies for the reaction of $H_2 + \cdot Si(OH)_3$, and these results are shown in Table 2. The important thing to note is that there is very little variation in the computed activation energy with improvements in the basis sets or with the inclusion of electron correlation. It seems very unlikely that making further improvements of this type will change the activation barrier out of the 0.7−0.8 eV range, which is still quite far from the experimental values.

It is also possible to compute the activation energy of the reverse, de-passivation reaction, in which a hydrogen atom picks

TABLE 2: Activation Energies

	$H_2 + \cdot Si(OH)_3$		$\cdot H + HSi(OH)_3$	
method (energy/geometry)	eV	kcal/mol	eV	kcal/mol
UHF(6-31G**)//UHF(6-31G**)	0.795	18.34	0.813	18.74
UHF(6-311G**)//UHF(6-31G**)	0.756	17.44	0.823	18.97
UHF(6-31G**++)/UHF(6-31G**)	0.871	20.09	0.809	18.65
UHF(6-31G**)//MP2(6-31G**)	0.786	18.13	0.810	18.68
UHF(6-31G**++)//MP2(6-31G**)	0.862	19.87	0.806	18.58
MP2(6-31G**)//UHF(6-31G**)	0.741	17.08	0.554	12.77
MP2(6-311G**)//UHF(6-31G**)	0.626	14.44	0.528	12.18
MP2(6-31G**++)/UHF(6-31G**)	0.802	18.50	0.536	12.36
MP2(6-31G**)//MP2(6-31G**)	0.747	17.22	0.554	12.77
MP2(6-31G**++)//MP2(6-31G**)	0.797	18.38	0.521	12.02

off the bound H to form H_2 and the dangling bond defect. The activation energies obtained for this process are shown in Table 2. Unlike the H_2 reaction, the activation energy for this reverse process changes significantly with the inclusion of electron correlation. To our knowledge, there has been no experimental determination of this quantity.

To explore the importance of using bigger clusters that include next-nearest neighbor effects, the model was expanded by adding another set of Si atoms, leading to the following reaction

$$H_2 + \cdot Si(OSiH_3)_3 \rightarrow \cdot H + HSi(OSiH_3)_3$$

At the UHF(6-31G**)//UHF(6-31G**) level of theory, using this larger cluster model had very little effect. The reaction energy changed from −0.017 to 0.004 eV (still an essentially energy neutral reaction). The H_2 reaction activation energy changed from 0.795 to 0.817 eV, and the H reaction activation energy did not change from the 0.813 eV value (cf. Table 2).

III. Dynamics

To calculate the "correct" activation energies the way it is done from experimental data, rate constants at different temperatures must be calculated for the process of interest. To extract values for the activation energy, the rate constant data is fit to the Arrhenius equation

$$k(T) = Ae^{-E_a/RT} \quad (1)$$

where E_a is the activation energy, A is referred to as the preexponential factor, and R is the Ideal Gas constant. This is the same fitting procedure that Li, et al. used to obtain their experimental rate constants.[3] If the natural logarithm is taken of both sides of the Arrhenius equation, the following expression is obtained

$$-\ln(k) = -\ln(A) + \frac{E_a}{R}\left(\frac{1}{T}\right) \quad (2)$$

This equation shows that if $-\ln(k)$ vs $1/T$ data is fit to a straight line, the slope gives the activation energy. To carry out this type of analysis, rate constants must be calculated for the reaction of interest.

The method chosen in this work for obtaining rate constants is the generalized transition state theory (GTST) of Truhlar and co-workers[14] using direct dynamics based on our previously computed ab initio data. A very brief outline of the method will be given in this section, with the main emphasis on the definition of the terms to be used. Detailed discussions and derivations of GTST can be found elsewhere.[14] All of the dynamics (rate constant) calculations presented here were done with the POLYRATE program.[15]

Conventional transition state theory (TST) calculates the thermal rate constants by assuming that all of the transition state species came directly from reactants and will be converted into products. The rate is then the flux across a surface in phase space in the product direction. This rate is given by

$$k(T) = \frac{\sigma\, Q(T)}{\beta h \Phi(T)} e^{-\beta V} \tag{3}$$

where β is $(k_B T)^{-1}$, h is Planck's constant, $Q(T)$ is the conventional transition state classical partition function with its zero of energy at the saddle point, $\Phi(T)$ is the reactant classical partition function with its zero of energy at the overall zero of energy, and V is the energy of the saddle point relative to the overall zero of energy. The generalized transition state theory rate constant, k^{GT}, is obtained by varying the position of the dividing surface along the minimum energy path to minimize the value of the computed rate constant.

$$k^{GT}(T) = \min k^{GT}(T,s) = k^{GT}(T,s^{CVT}(T)) \tag{4}$$

where

$$k^{GT}(T,s) = \frac{\sigma\, Q(T,s)}{\beta h\, \Phi(T)} e^{-\beta V_{MEP}(s)} \tag{5}$$

Results from this generalized treatment will be referred to as canonical variational theory (CVT). CVT corresponds to a maximum free energy of activation and includes both "entropic" and energetic effects and has been demonstrated to be more accurate than TST.

To obtain TST and CVT rate constants, all that is needed are the partition functions Q and Φ. In this work, the separable harmonic approximation is used, which neglects the couplings between the electronic, vibrational, and rotational energies. The partition function can then be written as

$$Q(T,s) = Q_{el}(T,s) Q_{vib}(T,s) Q_{rot}(T,s) \tag{6}$$

The formulas for each of these partition functions are discussed in detail in reference 13. Using only one electronic surface, Q_{el} depends on the degeneracy of the electronic state, Q_{vib} depends on the harmonic vibrational frequencies, and Q_{rot} depends on the moments of inertia. All of these quantities are easily calculated from the structural and energetic data discussed previously. TST rate constants can be computed solely from the results of calculations at the stationary points (reactants, products, and transition state). The CVT rate constants require information from additional points along the reaction path around the transition state.

The above two methods give a hybrid treatment of the rate constant, in that the motion in the degrees of freedom orthogonal to the reaction path are treated quantum mechanically, and the motion along the reaction path is treated classically, neglecting quantum tunneling effects. This means that for reactions involving hydrogen atoms k^{CVT} may underestimate the rate, particularly at low temperatures. Quantum reaction path effects can be included via a multiplicative transmission coefficient as

$$k^{CVT/G}(T) = \kappa^{G}(T) k^{CVT}(T) \tag{7}$$

The κ factor is calculated via

$$\kappa^{G}(T) = \frac{\int_0^\infty P^{G}(E) e^{-E/k_B T} dE}{\int_0^\infty \theta(E - V_a^*) e^{-E/k_B T} dE} \tag{8}$$

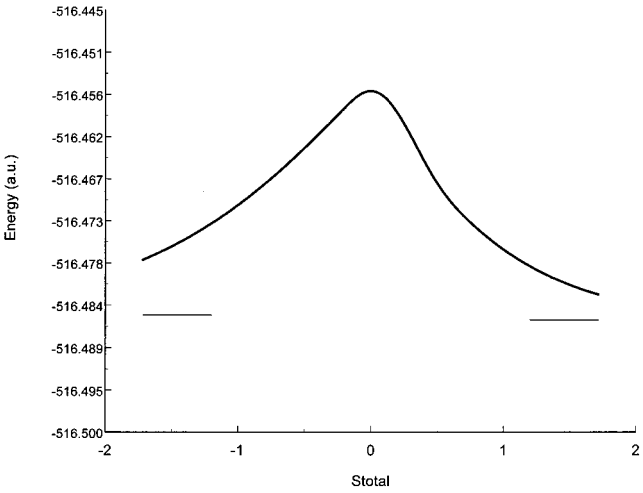

Figure 2. Potential energy curve along the intrinsic reaction coordinate (IRC). Stotal is equal to zero at the transition state, negative toward the reactants, and positive toward the products.

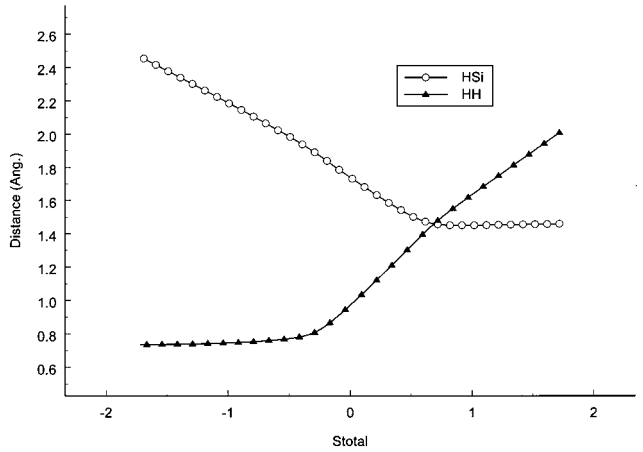

Figure 3. Distance changes during reaction. Stotal is the mass weighted distance and is equal to zero at the transition state, negative toward the reactants, and positive toward the products.

where $P^{G}(E)$ is the probability for the system with energy E to tunnel through the barrier, $\theta(E - V_a^*)$ is the unit step function at $x = 0$, and V_a^* is the minimum energy potential plus the vibrational zero point corrections. There are several methods for calculating $P^{G}(E)$ implemented in the POLYRATE program. The zero-curvature tunneling method,[16] ZCT, allows tunneling along the minimum energy path (MEP) only and requires the same information needed for the CVT calculation but over a much wider range of reaction coordinates. The centrifugal-dominant small-curvature semiclassical adiabatic ground-state method,[17] SCT, allows some deviation from the MEP (corner-cutting) and requires the same information as the ZCT method.

To perform the direct dynamics calculations, including tunneling as discussed above, many points along the intrinsic reaction coordinate, IRC (also know as MEP), are needed.[18] The large computational effort for direct dynamics comes from the fact that at each point along the IRC, the geometry, potential energy, energy gradient vector, and Hessian (energy second-derivative) matrix is needed. In the present study, 83 points were used along the UHF(6-31G**) IRC—the reactants, the products, the TS, and 40 points on each side of the TS. The potential energy along the IRC is shown in Figure 2. The reaction coordinate is a mass-weighted Cartesian coordinate and is arbitrarily set to + toward the reactants and to − toward the products. The IRC plots give a very nice picture of the height

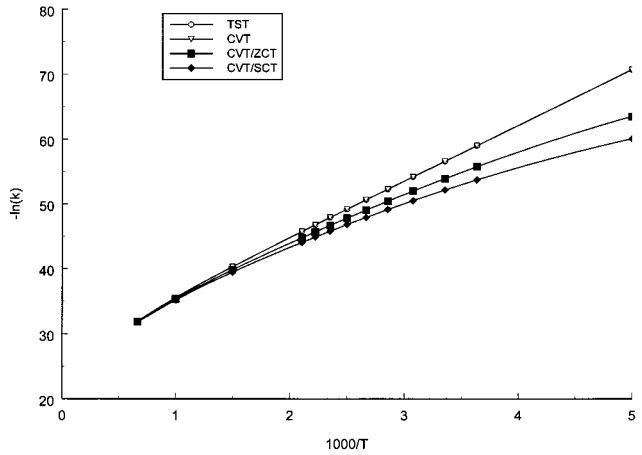

Figure 4. Arrhenius plot of $-\ln(k)$ vs $1/T$ from calculated rate constants.

TABLE 3: Rate Constants for $H_2 + \cdot Si(OH)_3$ (cm^3/molecule-sec)

T (K)	TST	CVT	CVT/ZCTT	CVT/SCT
100	4.98×10^{-50}	4.65×10^{-50}	2.84×10^{-34}	8.01×10^{-31}
200	1.96×10^{-31}	1.92×10^{-31}	2.48×10^{-28}	7.76×10^{-27}
298	2.63×10^{-25}	2.60×10^{-25}	3.68×10^{-24}	2.16×10^{-23}
400	4.31×10^{-22}	4.28×10^{-22}	1.67×10^{-21}	4.53×10^{-21}
667	3.16×10^{-18}	3.15×10^{-18}	4.98×10^{-18}	7.15×10^{-18}
1000	3.75×10^{-16}	3.74×10^{-16}	4.54×10^{-16}	5.33×10^{-16}
1500	1.33×10^{-14}	1.32×10^{-14}	1.43×10^{-14}	1.54×10^{-14}

TABLE 4: Activation Energies for H_2 Reaction

method	E_a (eV)	E_a (kcal/mol)
$E_{TS} - E_{reactants}$	0.80	18.34
$E_{TS} - E_{reactants}$ + ZPE	0.75	17.25
TST	0.75	17.19
CVT	0.75	17.20
CVT/ZCT	0.62	14.21
CVT/SCT	0.54	12.41
experiment	0.3−0.4	6.9−9.3

and width of the barrier for the reaction of interest. In addition to its use in direct dynamics, the IRC is the only way to verify that the TS calculated is the correct one for the reaction of interest by showing that it connects the reactants and products. Figure 3 shows how the H−H and H−Si distances vary along the IRC, indicating the loss of H_2 toward the right (indicating the correct reactants) and the loss of H toward the left (indicating the correct products).

Table 3 shows the rate constants for the reaction $H_2 + \cdot Si(OH)_3 \rightarrow \cdot H + HSi(OH)_3$, obtained from the TST, CVT, ZCT, and SCT methods at several sample temperatures. The k^{CVT} values are always slightly lower than the k^{TST} values. The $k^{CVT/ZCT}$ and $k^{CVT/SCT}$ values show that tunneling is indeed important at low temperatures, making an ~2 orders of magnitude increase in the rate at room temperature.

Figure 4 shows the calculated $-\ln(k)$ vs $1/T$ plots. Similar to the experimental data, the above curves are not actually straight lines over a wide range of temperature. Therefore, the value of the activation energy obtained from plots such as these clearly depends on the temperature range used to fit to the $-\ln(k)$ vs $1/T$ equation. It is most obvious in the CVT/ZCT and CVT/SCT plots that the slope of the line increases with increasing T (decreasing $1/T$), and the activation energy increases as a function of temperature. The experiments of Li et al.[3] used data over the temperature range of 23 to 299 °C (296−473 K). Therefore, for comparison, several calculations were done in the range 298−400 K to extract activation energy estimates. A summary of activation energy results obtained for the reaction of $H_2 + \cdot Si(OH)_3$ are shown in Table 4.

IV. Conclusions

From these results, it is clear that tunneling has a large effect on the computed activation energy and must be included to obtain reasonable results. The TST and CVT results are the same as that obtained from zero-point corrected barrier height calculations. The best direct dynamics estimate, CVT/SCT, of 0.54 eV is indeed smaller than the 0.75 eV value obtained only from the energetics of the stationary points on the potential energy surface but is still slightly larger than the 0.3−0.4 eV experimental quantity.

Two studies are currently underway to provide a more detailed and definitive examination of this problem. The first is to perform the same direct dynamics calculations, including tunneling, based on an MP2 IRC. This will provide a better potential with a good estimate of the reaction energy. The second calculation is to probe the adequacy of a cluster model for the condensed phase *a*-SiO_2 system. A typical E'_γ center (oxygen vacancy site) has a positive charge located nearby and a cage-like reaction site. Studies using a model of 106 atoms formed from a relaxed quartz structure with the O^- vacancy are underway.

Acknowledgment. H.A.K. acknowledges support through the Summer Faculty Fellowship program (RDL/AFOSR) and the Maui High Performance Computer Center. H.A.K. also acknowledges the support of the NSF for the computational chemistry program at the University of Memphis through Grant Nos. STI-9602656 (Academic Research Infrastructure program) and CHE-9708517 (Chemical Research Instrumentation and Facilities Program). We would like to thank Professors Bernard Kirtman and Arthur H. Edwards for many helpful discussions during this work.

References and Notes

(1) (a) Griscom, D. L. *J. Non-Cryst. Solids* **1985**, *73*, 51. (b) Conely, J. F.; Lenahan, P. M. A Review of Electron Spin Resonance Spectroscopy of Defects in Thin Film SiO_2 on Si. *Physics and Chemistry of SiO_2 and the Si/SiO_2 Interface III*; Massoud, H. Z., Poindexter, E. H., Helms, E. R., Eds.; Electrochemical Soc.: Pennington, NJ, 1996. (c) Edwards, A. H. Theory of Defects in the MOS system. *The Phyics and Chemistry of SiO_2 and the Si−SiO_2 Interface*; Helms, C. R., Deal, B. E., Eds.; Plenum Press: New York, 1988.

(2) Poindexter, E. H.; Caplan, P. J.; Geradi, G. J. *The Physics and Chemistry of SiO_2 and the Si−SiO_2 Interface*; Helms, C. R., Deal, B. E.; Plenum Press: New York, 1988; p 299.

(3) Li, Z.; Fonash, S. J.; Poindexter, E. H.; Harmatz, M.; Rong, F.; Buchwald, W. R. *J. Non-Cryst. Solids* **1990**, *126*, 173.

(4) Brower, K. L. *Phys. Rev.* **1988**, *B38*, 9657.

(5) Shelby, J. E. *J. Appl. Phys*. **1977**, *48*, 3387.

(6) Radzig, V. A.; Bqgratashvili, V. N.; Tsypina, V. I.; Chernov, P. V.; Ryboltovskii, A. O. *J. Phys. Chem.* **1995**, *99*, 6640.

(7) Edwards, A. H.; Pickard, J. A.; Stahlbush, R. E. *J. Non-Cryst. Solids* **1994**, *179*, 148.

(8) Edwards, A. H. *J. Non-Cryst. Solids* **1995**, *187*, 232.

(9) Ditchfield, R.; Hehre, W. J.; Pople, J. A. *J. Chem. Phys*. **1971**, *54*, 724; Hehre, W. J.; Ditchfield, R.; Pople, J. A. *J. Chem. Phys.* **1972**, *56*, 2257.

(10) Gordon, M. S. *Chem. Phys. Lett*. **1980**, *76*, 163.

(11) Schmidt, M. W.; Baldridge, K. K.; Boatz, J. A.; Elbert, S. T.; Gordon, M. S.; Jensen, J. H.; Koseki, S.; Matsunaga, N.; Nguyen, K. A.; Su, S. J.; Windus, T. L.; Dupuis, M.; Montgomery, J. A. *J. Comput. Chem.* **1993**, *14*, 1347.

(12) Frisch, M. J.; Trucks, G. W.; Schlegel, H. B.; Gill, P. M. W.; Johnson, B. G.; Robb, M. A.; Cheeseman, J. R.; Keith, T.; Petersson, G. A.; Montgomery, J. A.; Raghavachari, K.; Al-Laham, M. A.; Zakrzewski, V. G.; Ortiz, J. V.; Foresman, J. B.; Cioslowski, J.; Stefanov, B. B.;

Nanayakkara, A.; Challacombe, M.; Peng, C. Y.; Ayala, P. Y.; Chen, W.; Wong, M. W.; Andres, J. L.; Replogle, E. S.; Gomperts, R.; Martin, R. L.; Fox, D. J.; Binkley, J. S.; Defrees, D. J.; Baker, J.; Stewart, J. P.; Head-Gordon, M.; Gonzalez, C.; Pople, J. A. Gaussian 94, Revision E.2, Gaussian, Inc., Pittsburgh, PA, 1995.

(13) Allendorf, M. D.; Melius, C. F.; Ho, P.; Zachariah, M. R. *J. Phys. Chem.* **1995**, *99*, 15285.

(14) Truhlar, D. G.; Isaacson, A. D.; Garrett, B. C. Generalized Transition State Theory. *The Theory of Chemical Reaction Dynamics*; Baer, M., Ed.; CRC Press: Boca Raton, FL, 1985; Vol. 4, pp 65−137.

(15) Steckler, R.; Chuang, Y.-Y.; Fast, P. L.; Coitiño, E. L.; Corchado, J. C.; Hu, W.-P.; Liu, Y.-P.; Lynch, G. C.; Nguyen, K. A.; Jackels, C. F.; Gu, M. Z.; Rossi, I.; Clayton, S.; Melissas, V. S.; Garrett, B. C.; Isaacson, A. D.; Truhlar, D. G. POLYRATE Version 7.3.1, University of Minnesota, Minneapolis, 1997.

(16) Truhlar, D. G.; Kuppermann, A. *J. Am Chem. Soc*. **1971**, *93*, 1840.

(17) Liu, Y.-P.; Lynch, G. C.; Truong, T. N.; Lu, D.-H.; Truhlar, D. G.; Barrett, B. C. *J. Am. Chem. Soc*. **1993**, *115*, 2408.

(18) Baldridge, K. K.; Gordon, M. S.; Stechkler, R.; Truhlar, D. G. *J. Phys. Chem*. **1989**, *93*, 5107.